THE ASTROPHYSICAL JOURNAL, 219:31–45, 1978 January 1

THE VELOCITY FIELD OF THE BARRED SPIRAL GALAXY NGC 5383

CHARLES J. PETERSON, VERA C. RUBIN,* W. KENT FORD, JR.,* AND NORBERT THONNARD
Department of Terrestrial Magnetism, Carnegie Institution of Washington
Received 1977 May 9; accepted 1977 June 21

ABSTRACT

The velocity field of the barred spiral galaxy NGC 5383 has large-scale deviations from the pattern expected for only circular motions. Velocity gradients across the nucleus show a simple sinusoidal dependence on position angle, but the interpretation in terms of rotational and radial motions is dependent upon the adopted geometry of the galaxy. Exterior to the nucleus, the kinematics are more complex and are discussed in terms of two models. A likely model is that of a warped disk, which could be the result of a recent gravitational interaction with a nearby dwarf–barred spiral companion. For a warped-disk model, only rotational velocities are present in the nucleus. A second model interprets the observed velocities in terms of a rotating planar disk, in which case outward radial motions of ~ 180 km s^{-1} exist in the bar. Nuclear gas is both rotating and contracting [$V(R) = 136 \pm 10$ km s^{-1}, $E(R) = -60 \pm 10$ km s^{-1} at $R =$ 800 pc].

Observation of the integrated 21 cm neutral hydrogen emission shows an asymmetrical profile, with the maximum flux occurring at the systemic velocity of the companion. The asymmetry may be due to 21 cm radiation from hydrogen in the companion, to a nonuniform distribution of neutral hydrogen in NGC 5383, or to both. The total 21 cm integrated flux density, 16.7 Jy km s^{-1}, corresponds to a total hydrogen mass of $9 \times 10^9 \mathscr{M}_\odot$, and a $\mathscr{M}_{\rm HI}/L_{\rm opt}$ of 0.2 at an adopted distance of 50 Mpc. A comparison with the barred spiral NGC 3351 shows NGC 5383 to be more luminous and bluer, and to have a higher hydrogen mass and higher angular momentum.

Subject headings: galaxies: individual — galaxies: internal motions — radio sources: 21 cm radiation

I. INTRODUCTION

NGC 5383 [$\alpha(1950) = 13^{\rm h}55^{\rm m}.0$, $\delta = +42°5'$] is one of the few bright barred spiral galaxies (type SBb, luminosity class II, $m_{\rm pg} = 12.5$) in the northern sky. It has a bright nucleus, a prominent bar in position angle (P.A.) 134°, and faint spiral arms. The nuclear region consists of three almost parallel bright condensations elongated in position angle 109°; the two well-defined absorption lanes which divide the nuclear region merge into the dust lanes along the bar. The outer structure of the galaxy is noticeably asymmetrical; the arm which curves to the southwest is broader and extends over a longer arc than the arm on the opposite side of the galaxy (Figs. 1 and 2, Plates 1, 2, and 3).

Lynds (1972, 1974) has published an Hα narrowband photograph which shows the strong nuclear emission. On very deep exposures (Fig. 2*a*), filamentary material fills in much of the region surrounding the bar, causing the galaxy to resemble a two-armed nonbarred galaxy. Sandage (1961) has earlier noted the resemblance of NGC 5383 to the nonbarred spiral M83.

Pease (1917) stated that "some disturbance has altered the regularity of distribution" of the surface luminosity of the object, and he noted the existence of a faint, very low-surface-brightness companion spiral 3'.1 to the south (Fig. 2). We show below that the companion galaxy has a velocity close to that of NGC 5383, which makes it likely that the two form an interacting pair. The companion (MCG 7-29-22 = UGC 8877) is classified SBdm by Nilson (1973); we will hereafter call it NGC 5383a.

The distribution of galaxies in the area around NGC 5383 suggests that it may be a member of a loose cluster. Four of these galaxies (A1349+40, NGC 5353, NGC 5354, and NGC 5371) have velocities in the Second Reference Catalog of Bright Galaxies (de Vaucouleurs, de Vaucouleurs, and Corwin 1976) with a mean V_0(corrected) $= 2583 \pm 205$ km s^{-1}, while for NGC 5383, $V_0 = 2365$ km s^{-1}. We adopt a distance of 50 Mpc for NGC 5383 and the group, corresponding to $H \approx 50$ km s^{-1} Mpc^{-1}. At this distance, $1'' = 242$ pc.

In § II we describe our optical and 21 cm observations of NGC 5383. Section III discusses the spatial orientation of the galaxy and presents the velocity field. Two interpretations, one involving a warped disk and one including streaming motions in a plane, are given in § IV. A comparison with the barred spiral NGC 3351 and conclusions are in §§ V and VI.

* Visiting Astronomer, Kitt Peak National Observatory, which is operated by the Association of Universities for Research in Astronomy, Inc., under contract with the National Science Foundation; and Visiting Astronomer, Lowell Observatory.

TABLE 1

Record of Spectroscopic Observations for NGC 5383

Plate	Telescope	Date	Dispersion (Å mm^{-1})	Exposure (minutes)	Position Number	Position Angle (degrees)	Lines Measured
DTM-2144B....	2.1 m	1972 May 16	139	29	3	240, through nucleus	Hα
K-2515A.......	2.1 m	1974 Mar 22	123	60	6	90, through nucleus	Hα, Hβ, [N II], [S II]
4M-107........	4 m	1974 Mar 14	54	60	6	90, through nucleus	Hα, [N II], [S II]
4M-111........	4 m	1974 Mar 17	54	120	5	90, northwest arm	Hα, [N II], [S II]
4M-115........	4 m	1974 Mar 18	54	180	8	90, southeast arm	Hα, [N II]
4M-802........	4 m	1975 May 3	52	60	9	109, through nucleus	Hα, [N II], [S II]
4M-803........	4 m	1975 May 3	52	60	10	109, offset southwest	Hα, [N II], [S II]
4M-804A.......	4 m	1975 May 3	52	20	9	109, through nucleus	Hα, [N II], [S II]
4M-804B.......	4 m	1975 May 3	52	60	7	109, offset northeast	Hα, [N II], [S II]
4M-805A.......	4 m	1975 May 3	52	48	2	63, northwest arm	Hα, [N II], [S II]
4M-808A.......	4 m	1975 May 4	52	107	2	63, northwest arm	Hα, [N II], [S II]
4M-809A.......	4 m	1975 May 4	52	85	11	134, offset southwest	Hα, [N II], [S II]
4M-809B.......	4 m	1975 May 4	52	60	1	186, through nucleus	Hα, [N II], [S II]
4M-811B.......	4 m	1975 May 5	49	90	11	134, offset southwest	Hβ, Hγ, Hδ, Hε, [O III]
4M-812........	4 m	1975 May 5	52	120	4	45, southeast arm	Hα, [N II], [S II]
4M-813........	4 m	1975 May 5	52	90	...	156, along bar of companion	Hα

II. OBSERVATIONAL DATA

a) *The Optical Observations*

Optical spectra at high spatial and high-velocity resolution have been obtained by using a two-stage Carnegie image-tube spectrograph at the 1.8 m Perkins telescope of Ohio Wesleyan and Ohio State Universities at Lowell Observatory, and at the 2.1 m and 4 m telescopes at Kitt Peak National Observatory. Previous optical studies of this galaxy at lower dispersion and scale were made by Burbidge, Burbidge, and Prendergast (1962) and Cheriguene (1975). The measured spectra are listed in Table 1; slit positions are shown in Figure 1. Figure 2*a* shows a light print of NGC 5383 to emphasize the dust pattern and a dark print to show the outer extent of the spiral pattern. Figure 2*b* is a reproduction of NGC 5383 and its companion from the Palomar Sky Survey, with the position of the slit shown for the companion. Representative spectra showing emission lines in the red are illustrated in Figure 3 (Plates 4, 5) for the arms, the bar, and the nucleus. Note the various inclinations of the emission features arising in individual knots near the nucleus. These imply either streaming motions in each knot or nonaligned rotation axes for the individual regions.

In the nucleus and arms, the relative emission-line intensities are as follows: $I(\mathrm{H}\alpha) > I([\mathrm{N\,II}])$, $I([\mathrm{S\,II}]\,\lambda6717) > I([\mathrm{S\,II}]\lambda6731)$, and $I([\mathrm{O\,II}])\lambda3726 < I([\mathrm{O\,II}]\lambda3729)$. The [O II] and [S II] intensities imply a low electron density. Balmer lines Hα through Hδ are observed in emission, with surrounding broader Balmer absorption in the stellar continuum at Hβ, Hγ, and Hδ. Hε is also present in emission in the broad Ca II H absorption line. [O III] is weakly present. This pattern of intensities is similar to that observed in low excitation nebulae. Absorption lines typical of a solar type spectrum are visible, with Cr I λ4666, Fe I λ4383, Fe I λ4325, Ca I λ4226, and Ca II H and K especially prominent. This integrated spectrum indicates a significant late-type stellar population, while the Balmer lines in absorption indicate an enhanced younger stellar population.

Velocities from the emission lines have been measured on a Mann two-coordinate measuring machine and are tabulated in Table 2. The symmetrical pattern of velocities in P.A. 109° through the nucleus is illustrated in Figure 4*a*. Velocities through the emission knots along the bar, but offset 7″ SW of the nucleus, are shown in Figure 4*b*. The pronounced asymmetry of the rotation curve parallel to the axis of the bar can be seen clearly, and is an indication of the strong velocity gradients which are present across the bar. There is only fair agreement with the overall velocity data of Burbidge, Burbidge, and Prendergast (1962), but good agreement with those of Cheriguene (1975) when those velocities are all increased by $+45\ \mathrm{km\ s^{-1}}$.

Because the complex morphology and velocity field of NGC 5383 could be the result of an encounter with a second galaxy, we have obtained a spectrum of the companion NGC 5383a. For NGC 5383, $V = 2264 \pm 20\ \mathrm{km\ s^{-1}}$; for NGC 5383a, $V = 2379 \pm 20\ \mathrm{km\ s^{-1}}$; this makes it likely that the two form a dynamically interacting pair.

b) *The Radio Observations*

NGC 5383 was observed at 21 cm with the NRAO 91.4 m transit radio telescope[1] in 1975 September. The integrated profile shown in Figure 5 represents 54 minutes' integration in both polarizations with a beam 10′.3 × 11′.3. The integrated flux density is $S_\nu = 16.7 \pm 2.0$ Jy km s^{-1}. The total hydrogen mass (Roberts 1962) at the adopted distance of 50 Mpc is

$$\mathscr{M}_{\mathrm{H\,I}}/M_\odot = 2.36 \times 10^5 D^2 \int S_\nu dV$$
$$= 9.9 \times 10^9\ \mathscr{M}_\odot\,,$$

where D is the distance in Mpc. However, this must

[1] Operated by Associated Universities, Inc., under contract with the National Science Foundation.

1978ApJ...219...31P

TABLE 2

HELIOCENTRIC VELOCITIES FOR SPECTRA OF NGC 5383

2144B		P. A. 240		
LINE		X *	Y *	V
Hα	6562	-4.1	2.4	2419
		-1.2	0.7	2304
		0.9	-0.5	2138
		5.0	-2.9	2206
		7.8	-4.5	2100

K-2515A		P. A. 90		
LINE		X	Y	V
Hβ	4861	-7.0	0.0	2346
		-3.8	0.0	2281
		0.0	0.0	2259
		6.1	0.0	2142
		10.7	0.0	2101
[NII]	6548	-5.9	0.0	2324
		0.2	0.0	2221
		6.7	0.0	2181
Hα	6562	-10.0	0.0	2363
		-5.6	0.0	2316
		-0.0	0.0	2238
		6.6	0.0	2148
		12.1	0.0	2131
[NII]	6583	-8.4	0.0	2343
		-4.3	0.0	2319
		0.3	0.0	2225
		6.3	0.0	2142
		11.7	0.0	2132
[SII]	6716	-5.0	0.0	2329
		0.6	0.0	2260
		6.6	0.0	2192
[SII]	6730	-6.2	0.0	2314
		-0.2	0.0	2255
		5.7	0.0	2177

4M-107		P. A. 90		
LINE		X	Y	V
[NII]	6548	0.0	0.0	2171
Hα	6562	-16.1	0.0	2369
		-13.6	0.0	2335
		-11.1	0.0	2355
		-8.7	0.0	2358
		-6.2	0.0	2285
		-3.7	0.0	2205
		-1.2	0.0	2168
		1.2	0.0	2173
		3.6	0.0	2166
		0.0	0.0	2172
[NII]	6583	-13.6	0.0	2336
		-11.1	0.0	2344
		-8.6	0.0	2359
		-6.2	0.0	2303
		-3.7	0.0	2214
		-1.2	0.0	2176
		1.2	0.0	2156
		0.0	0.0	2168
[SII]	6716	0.0	0.0	2168
[SII]	6730	0.0	0.0	2165

4M-111		P. A. 90		
LINE		X	Y	V
[NII]	6548	2.6	28.0	2164
Hα	6562	6.9	28.0	2280
		38.2	28.0	2183
		40.9	28.0	2140
		43.3	28.0	2169
[NII]	6583	2.6	28.0	2163
[SII]	6716	2.6	28.0	2175
[SII]	6730	2.6	28.0	2172

4M-115		P. A. 90		
LINE		X	Y	V
Hα	6562	-48.2	-21.4	2413
		-44.8	-21.4	2374
		-42.2	-21.4	2369
		-36.7	-21.4	2366
		-30.9	-21.4	2314
[NII]	6583	-41.6	-21.4	2373
		-30.9	-21.4	2316

4M-802		P. A. 109		
LINE		X	Y	V
[NII]	6548	11.7	4.0	2194
		9.3	3.2	2206
		7.0	2.4	2192
		4.7	1.6	2194
		2.3	0.8	2195
		-2.3	-0.8	2338
		-4.7	-1.6	2337
		-7.0	-2.4	2314
Hα	6562	57.7	19.9	2169
		55.3	19.0	2165
		53.0	18.2	2162
		50.6	17.4	2139
		48.3	16.6	2095
		23.4	8.0	2110
		21.0	7.2	2125
		18.7	6.4	2142
		16.4	5.6	2142
		14.0	4.8	2170
		11.6	4.0	2183
		9.3	3.2	2203
		7.0	2.4	2183
		4.6	1.6	2191
		2.3	0.8	2208
		-2.3	-0.8	2340
		-4.7	-1.6	2357
		-7.0	-2.4	2339
		-9.3	-3.2	2320
		-19.7	-6.8	2370
		-22.1	-7.6	2394
		-24.4	-8.4	2419
		-46.5	-16.0	2425
		-48.8	-16.8	2394
[NII]	6583	57.6	19.8	2174
		23.3	8.0	2102
		21.0	7.2	2145
		18.7	6.4	2147
		16.3	5.6	2155
		14.0	4.8	2201
		11.7	4.0	2194
		9.4	3.2	2208
		6.8	2.3	2200
		4.4	1.5	2210
		2.1	0.7	2199
		-2.6	-0.9	2364
		-4.9	-1.7	2366
		-7.2	-2.5	2341
		-9.6	-3.3	2320
		-19.6	-6.7	2378
		-21.9	-7.6	2380
		-24.4	-8.4	2381
		-48.2	-16.6	2356
[SII]	6716	57.1	19.7	2135
		16.3	5.6	2173
		14.0	4.8	2194
		11.7	4.0	2202
		9.3	3.2	2201
		7.0	2.4	2200
		4.7	1.6	2196
		2.3	0.8	2188
		-2.3	-0.8	2350
		-4.7	-1.6	2349
		-7.0	-2.4	2300
[SII]	6730	57.0	19.6	2143
		11.7	4.0	2179
		9.3	3.2	2182
		7.0	2.4	2212
		4.7	1.6	2206
		2.3	0.8	2216
		-2.3	-0.8	2337
		-4.7	-1.6	2352
		-7.0	-2.4	2331

4M-803		P. A. 109		
LINE		X	Y	V
[NII]	6548	11.8	-1.2	2117
		10.1	-1.8	2134
		8.1	-2.4	2130
		5.6	-3.3	2133
		3.0	-4.2	2157
		-0.8	-5.5	2208
		-30.5	-15.7	2321
		-42.0	-19.7	2386
Hα	6562	59.6	15.3	2100
		20.8	1.9	2112
		17.2	0.7	2093
		15.0	-0.1	2088
		13.0	-0.8	2095
		10.7	-1.5	2117

4M-803		CONTINUED		
LINE		X	Y	V
		8.6	-2.3	2129
		5.7	-3.3	2136
		2.5	-4.4	2154
		-0.9	-5.6	2205
		-25.0	-13.8	2317
		-27.5	-14.7	2342
		-29.5	-15.4	2361
		-31.3	-16.0	2351
		-38.6	-18.5	2377
		-41.4	-19.5	2374
		-44.2	-20.5	2371
		-47.7	-21.6	2377
[NII]	6583	20.7	1.9	2117
		15.0	-0.1	2065
		12.7	-0.9	2106
		10.6	-1.6	2126
		7.4	-2.7	2133
		5.2	-3.4	2142
		2.4	-4.4	2156
		-1.0	-5.6	2203
		-27.4	-14.6	2322
		-29.6	-15.4	2344
		-31.4	-16.1	2347
		-39.5	-18.8	2342
		-42.2	-19.8	2373
		-44.4	-20.5	2378
		-47.6	-21.6	2373
[SII]	6716	11.4	-1.3	2121
		9.1	-2.1	2142
		6.3	-3.1	2151
		3.0	-4.2	2152
		-31.2	-16.0	2349
		-41.1	-19.4	2360
		-42.9	-20.0	2377
		-44.8	-20.6	2382
		-47.9	-21.7	2359
[SII]	6730	11.3	-1.3	2121
		8.4	-2.4	2138
		6.2	-3.1	2153
		-31.2	-16.0	2361
		-41.8	-19.6	2370
		-43.8	-20.3	2378

4M-804A		P. A. 109		
LINE		X	Y	V
[NII]	6548	7.0	2.4	2171
		4.7	1.6	2184
		2.3	0.8	2198
		-0.0	-0.0	2286
		-2.3	-0.8	2332
		-4.7	-1.6	2335
Hα	6562	58.0	20.0	2144
		49.3	17.0	2073
		18.7	6.4	2133
		16.3	5.6	2172
		14.0	4.8	2172
		11.7	4.0	2172
		9.4	3.2	2183
		7.0	2.4	2183
		4.7	1.6	2183
		2.3	0.8	2210
		0.0	0.0	2262
		-2.3	-0.8	2335
		-4.6	-1.6	2346
		-7.0	-2.4	2327
		-22.0	-7.6	2390
[NII]	6583	9.4	3.2	2190
		7.0	2.4	2198
		4.7	1.6	2189
		2.3	0.8	2197
		0.0	0.0	2247
		-2.3	-0.8	2340
		-4.7	-1.6	2326
		-7.0	-2.4	2319
[SII]	6716	9.3	3.2	2179
		7.0	2.4	2195
		4.7	1.6	2185
		2.3	0.8	2202
		0.0	0.0	2275
		-2.3	-0.8	2329
		-4.7	-1.6	2364
[SII]	6730	7.0	2.4	2189
		4.6	1.6	2188
		2.3	0.8	2196
		0.0	0.0	2343
		-2.3	-0.8	2363
		-4.7	-1.6	2386

* X and Y form a Cartesian coordinate system on the plane of the sky, centered on the nucleus, with X positive in the west direction, Y positive to the north.

TABLE 2 -- CONTINUED

4M-804B		P. A. 109		
LINE		X	Y	V
[NII]	6548	35.3	22.3	2187
Hα	6562	56.3	29.5	2207
		54.0	28.7	2176
		51.6	27.9	2155
		49.3	27.1	2149
		47.0	26.3	2157
		44.6	25.5	2175
		42.3	24.7	2175
		39.9	23.9	2174
		37.6	23.1	2186
		35.3	22.3	2201
		18.9	16.6	2276
		16.6	15.8	2264
		14.3	15.0	2266
		11.9	14.2	2299
		9.6	13.4	2303
		7.3	12.6	2331
		4.9	11.8	2348
		2.6	11.0	2360
		0.3	10.2	2370
		-2.1	9.4	2381
		-4.4	8.6	2397
		-6.8	7.8	2416
[NII]	6583	35.4	22.3	2218
		18.9	16.6	2306
		16.6	15.8	2297
		11.9	14.2	2291
		9.6	13.4	2287
		7.3	12.6	2313
		4.9	11.8	2336
		2.6	11.0	2351
		0.3	10.2	2375
		-2.1	9.4	2398
		-4.4	8.6	2400
		-6.8	7.8	2402
[SII]	6716	35.2	22.3	2209
		4.9	11.8	2368
		2.6	11.0	2367
		0.2	10.2	2373
		-2.1	9.4	2377
		-4.4	8.6	2391
[SII]	6730	35.3	22.3	2215
		0.2	10.2	2371
		-2.1	9.4	2385

4M-805A		P. A. 63		
LINE		X	Y	V
[NII]	6548	44.2	27.5	2136
		43.3	27.9	2136
		42.2	28.5	2141
Hα	6562	47.5	25.8	2161
		45.3	26.9	2150
		43.1	28.0	2139
		40.9	29.2	2137
		38.7	30.3	2158
		36.5	31.4	2164
		34.3	32.5	2203
		32.1	33.6	2238
		29.9	34.7	2242
		27.7	35.9	2221
		25.5	37.0	2226
		23.3	38.1	2216
		21.1	39.2	2223
		18.9	40.4	2226
		16.7	41.5	2249
		14.5	42.6	2258
		12.3	43.7	2246
		10.1	44.8	2257
		7.9	46.0	2298
		5.7	47.1	2292
		3.5	48.2	2307
		1.3	49.3	2326
		-11.9	56.0	2298
		-14.1	57.2	2315
[NII]	6583	44.6	27.3	2153
		42.8	28.2	2129
		41.2	29.0	2137
		38.6	30.3	2186
[SII]	6716	44.0	27.6	2154
		43.0	28.1	2154
		41.8	28.7	2136
		39.1	30.0	2162
[SII]	6730	44.1	27.5	2158
		43.0	28.1	2151
		41.8	28.7	2153
		38.7	30.3	2169

4M-808A		P. A. 63		
LINE		X	Y	V
[NII]	6548	43.1	28.0	2147
		40.9	29.2	2161
		38.7	30.3	2167
		36.5	31.4	2170
		29.9	34.8	2208
		27.7	35.9	2212
		25.5	37.0	2213
		23.3	38.1	2235
		21.1	39.2	2224
Hα	6562	45.3	26.9	2141
		43.1	28.0	2160
		40.9	29.2	2150
		38.7	30.3	2161
		36.5	31.4	2164
		34.3	32.5	2191
		32.1	33.6	2223
		29.9	34.8	2238
		27.7	35.9	2219
		25.4	37.0	2219
		23.3	38.1	2224
		21.1	39.2	2227
		18.9	40.4	2233
		16.7	41.5	2257
		14.5	42.6	2263
		12.3	43.7	2256
		10.1	44.8	2280
		7.8	46.0	2286
		5.7	47.1	2274
		3.5	48.2	2283
		-0.9	50.4	2328
		-3.1	51.6	2279
		-9.7	55.0	2291
		-12.0	56.1	2295
		-14.2	57.2	2311
		-16.3	58.3	2293
[NII]	6583	45.2	27.0	2142
		43.1	28.0	2155
		40.9	29.1	2152
		38.7	30.3	2168
		36.5	31.4	2172
		32.1	33.6	2246
		29.8	34.8	2252
		27.6	35.9	2226
		25.5	37.0	2230
		23.3	38.1	2239
		21.1	39.3	2245
		18.9	40.4	2248
		14.4	42.6	2256
		12.3	43.7	2267
		10.1	44.9	2275
		-9.7	55.0	2274
		-11.9	56.1	2291
[SII]	6716	43.1	28.0	2150
		40.9	29.1	2152
		38.7	30.3	2180
		36.5	31.4	2184
		34.3	32.5	2212
		32.1	33.6	2243
		29.8	34.8	2243
		27.7	35.9	2217
		25.4	37.0	2230
		23.3	38.1	2235
		21.1	39.3	2237
		18.9	40.4	2232
		12.3	43.7	2246
		10.1	44.8	2276
		-9.7	55.0	2322
		-12.0	56.1	2313
		-14.2	57.2	2317
[SII]	6730	43.1	28.0	2155
		40.9	29.2	2166
		38.7	30.3	2189
		36.5	31.4	2196
		32.1	33.6	2234
		29.8	34.8	2229
		27.7	35.9	2243
		25.5	37.0	2253
		23.3	38.1	2248
		21.1	39.2	2232
		18.9	40.4	2252

4M-809A		P. A. 134		
LINE		X	Y	V
[NII]	6548	42.3	32.4	2143
		33.4	23.8	2184
		31.6	22.1	2173
		29.8	20.4	2169
		28.1	18.7	2169

4M-809A		CONTINUED		
LINE		X	Y	V
		26.3	17.0	2179
		24.5	15.3	2198
		22.7	13.5	2188
		10.3	1.5	2138
		8.5	-0.2	2124
		6.8	-1.9	2117
		5.0	-3.6	2123
		3.2	-5.3	2159
		1.4	-7.0	2181
		-27.0	-34.5	2277
		-28.8	-36.2	2310
Hα	6562	51.2	41.0	2130
		49.4	39.3	2137
		47.6	37.6	2150
		45.8	35.8	2156
		44.1	34.1	2156
		42.3	32.4	2145
		40.5	30.7	2149
		38.8	29.0	2146
		37.0	27.3	2165
		35.2	25.6	2178
		33.4	23.8	2189
		31.6	22.1	2175
		29.8	20.4	2167
		28.0	18.7	2154
		26.3	17.0	2166
		24.5	15.3	2143
		22.7	13.5	2125
		19.2	10.1	2127
		17.4	8.4	2119
		15.7	6.7	2111
		13.9	5.0	2109
		12.1	3.2	2102
		10.3	1.5	2118
		8.5	-0.2	2126
		6.8	-1.9	2127
		5.0	-3.6	2103
		3.2	-5.3	2106
		1.4	-7.0	2113
		-0.4	-8.8	2159
		-5.7	-13.9	2211
		-18.1	-25.9	2256
		-19.9	-27.6	2257
		-25.2	-32.8	2294
		-27.0	-34.5	2297
		-28.8	-36.2	2319
		-30.5	-37.9	2337
		-32.3	-39.6	2348
		-34.1	-41.3	2330
		-35.9	-43.1	2341
[NII]	6583	47.6	37.6	2124
		45.8	35.8	2162
		44.1	34.1	2157
		42.3	32.4	2164
		40.5	30.7	2160
		38.7	29.0	2166
		36.9	27.2	2183
		35.2	25.6	2200
		33.4	23.8	2209
		31.6	22.1	2195
		29.8	20.4	2184
		28.1	18.7	2164
		26.3	17.0	2166
		24.5	15.3	2167
		22.7	13.5	2137
		21.0	11.8	2138
		19.2	10.1	2134
		17.4	8.4	2142
		15.6	6.7	2096
		13.8	4.9	2078
		10.3	1.5	2103
		8.5	-0.2	2114
		6.8	-1.9	2112
		5.0	-3.6	2116
		3.2	-5.3	2114
		1.4	-7.0	2145
		-0.4	-8.8	2150
		-25.2	-32.8	2283
		-27.0	-34.5	2297
		-28.8	-36.2	2317
		-30.6	-37.9	2339
		-32.3	-39.6	2351
		-34.1	-41.4	2356
[SII]	6716	44.1	34.1	2176
		42.3	32.4	2173
		40.5	30.7	2171
		38.7	29.0	2158
		36.9	27.2	2170
		35.2	25.6	2188
		33.4	23.8	2214

TABLE 2 -- Conclusion

4M-809A CONTINUED

LINE	X	Y	V
	31.6	22.1	2183
	29.8	20.4	2161
	28.1	18.7	2176
	26.4	17.0	2177
	24.5	15.2	2190
	13.8	5.0	2102
	10.2	1.4	2133
	8.5	-0.2	2126
	6.8	-1.9	2134
	5.0	-3.6	2130
	3.2	-5.3	2132
	1.4	-7.0	2148
	-27.0	-34.5	2314
	-28.8	-36.2	2337
	-30.5	-37.9	2346
	-32.3	-39.6	2342
	-34.1	-41.3	2349
[SII] 6730	43.6	33.7	2160
	41.8	32.0	2161
	40.1	30.3	2164
	37.3	27.6	2163
	35.6	26.0	2193
	33.8	24.2	2186
	32.0	22.5	2194
	30.3	20.8	2184
	28.5	19.1	2186
	26.7	17.4	2161
	10.7	1.9	2128
	9.0	0.2	2122
	7.2	-1.5	2116
	5.4	-3.2	2111
	3.6	-4.9	2105
	-26.6	-34.1	2297
	-28.3	-35.8	2321
	-30.1	-37.5	2345
	-31.9	-39.2	2377
	-33.7	-40.9	2371

4M-809B P. A. 186

LINE	X	Y	V
[NII] 6548	-0.5	4.9	2235
	-0.2	2.4	2255
	0.2	-2.4	2252
	0.5	-4.9	2225
Hα 6562	-6.2	58.6	2317
	-6.0	56.7	2315
	-1.3	12.3	2387
	-1.0	9.8	2359
	-0.8	7.4	2350
	-0.5	4.9	2257
	-0.2	2.4	2244
	0.2	-2.4	2233
	0.5	-4.9	2216
	0.8	-7.3	2163
	1.0	-9.8	2168
	1.3	-12.2	2206
	2.7	-25.4	2165
	3.4	-32.7	2186
	4.5	-42.5	2184
	5.1	-48.5	2225
[NII] 6583	-1.3	12.3	2345
	-1.0	9.8	2326
	-0.8	7.4	2324
	-0.5	4.9	2279
	-0.2	2.4	2242
	0.2	-2.4	2240
	0.5	-4.9	2224
	0.8	-7.4	2157
	1.0	-9.8	2152
[SII] 6716	-1.0	9.8	2357
	-0.5	4.9	2300
	-0.2	2.4	2272
	0.2	-2.4	2267
	0.5	-4.9	2206
[SII] 6730	-0.5	4.9	2266
	-0.2	2.4	2270
	0.2	-2.5	2247
	0.5	-4.9	2231

4M-811B P. A. 134

LINE	X	Y	V
Hε 3970	47.6	37.6	2186
	45.8	35.9	2170
	36.0	26.4	2188
	12.1	3.2	2089
	10.3	1.5	2114

4M-811B CONTINUED

LINE	X	Y	V
	-23.5	-31.1	2356
	-25.2	-32.8	2359
	-27.0	-34.5	2377
Hδ 4101	47.6	37.6	2168
	45.8	35.9	2144
	44.0	34.1	2145
	13.8	5.0	2076
	12.1	3.2	2057
	10.4	1.6	2064
	8.5	-0.2	2017
	-23.4	-31.1	2277
	-25.2	-32.8	2292
	-27.0	-34.5	2312
	-28.8	-36.2	2350
	-30.6	-37.9	2422
Hγ 4340	49.4	39.3	2160
	47.6	37.6	2165
	45.8	35.9	2115
	44.0	34.1	2109
	42.3	32.4	2133
	38.7	29.0	2164
	37.0	27.3	2181
	35.2	25.5	2190
	33.4	23.8	2183
	31.6	22.1	2153
	29.8	20.4	2154
	28.0	18.7	2187
	13.8	5.0	2039
	12.1	3.2	2067
	10.3	1.5	2100
	8.5	-0.2	2083
	6.7	-1.9	2084
	-23.5	-31.1	2299
	-25.2	-32.8	2293
	-27.0	-34.5	2332
	-28.8	-36.2	2354
	-30.5	-37.9	2358
	-32.3	-39.6	2313
Hβ 4861	49.4	39.3	2188
	47.6	37.6	2196
	45.8	35.8	2131
	44.0	34.1	2126
	42.2	32.4	2168
	40.5	30.7	2156
	38.7	29.0	2199
	36.9	27.3	2192
	35.2	25.6	2187
	33.4	23.8	2194
	31.6	22.1	2207
	29.8	20.4	2202
	13.8	5.0	2108
	12.1	3.2	2119
	10.3	1.5	2131
	8.5	-0.2	2135
	6.7	-1.9	2143
	-21.7	-29.4	2276
	-23.5	-31.1	2311
	-25.2	-32.8	2312
	-27.0	-34.5	2317
	-28.8	-36.2	2314
	-30.6	-37.9	2315
	-32.3	-39.6	2335
[OIII] 4958	-25.2	-32.8	2351
	-27.0	-34.5	2349
[OIII] 5006	47.6	37.6	2140
	45.8	35.8	2161
	12.1	3.2	2177
	10.3	1.5	2183
	8.5	-0.2	2225
	-23.5	-31.1	2339
	-25.2	-32.8	2336
	-27.0	-34.5	2330
	-28.8	-36.2	2333
	-30.6	-37.9	2343

4M-812 P. A. 45

LINE	X	Y	V
[NII] 6548	-42.1	-22.9	2379
	-40.4	-24.6	2395
	-38.6	-26.4	2374
	-22.9	-42.1	2342
	-21.2	-43.8	2323
	-19.4	-45.6	2320
	-17.7	-47.3	2313
	-15.9	-49.1	2310
	-14.2	-50.8	2302
	-12.4	-52.6	2270
	-10.7	-54.3	2266

4M-812 CONTINUED

LINE	X	Y	V
Hα 6562	-61.3	-3.7	2422
	-59.6	-5.4	2410
	-52.6	-12.4	2401
	-49.1	-15.9	2436
	-47.4	-17.6	2430
	-45.6	-19.4	2424
	-43.9	-21.1	2405
	-42.1	-22.9	2396
	-40.4	-24.6	2381
	-38.6	-26.4	2378
	-36.9	-28.1	2370
	-35.1	-29.8	2374
	-33.4	-31.6	2358
	-31.6	-33.3	2360
	-29.9	-35.1	2356
	-28.2	-36.8	2355
	-26.4	-38.6	2352
	-24.6	-40.4	2329
	-22.9	-42.1	2323
	-21.2	-43.8	2324
	-19.4	-45.6	2319
	-17.7	-47.3	2322
	-15.9	-49.1	2309
	-14.2	-50.8	2300
	-12.4	-52.6	2294
	-10.7	-54.3	2289
	-8.9	-56.1	2286
[NII] 6583	-60.4	-4.6	2403
	-58.7	-6.3	2384
	-48.2	-16.8	2462
	-46.5	-18.5	2441
	-44.7	-20.3	2419
	-43.0	-22.0	2405
	-41.2	-23.8	2403
	-39.5	-25.5	2396
	-37.8	-27.2	2383
	-36.0	-29.0	2368
	-34.3	-30.7	2357
	-32.5	-32.5	2356
	-30.8	-34.2	2344
	-29.0	-36.0	2349
	-27.3	-37.7	2347
	-25.5	-39.5	2332
	-23.8	-41.2	2327
	-22.0	-42.9	2319
	-20.3	-44.7	2327
	-18.6	-46.4	2317
	-16.8	-48.2	2315
	-15.1	-49.9	2300
	-13.3	-51.7	2290
	-11.6	-53.4	2288
	-9.8	-55.2	2283
[SII] 6716	-60.4	-4.6	2413
	-46.5	-18.5	2402
	-43.0	-22.0	2413
	-41.2	-23.8	2400
	-39.5	-25.5	2392
	-37.7	-27.2	2388
	-36.0	-29.0	2383
	-29.0	-36.0	2345
	-27.3	-37.7	2336
	-25.5	-39.5	2351
	-23.8	-41.2	2333
	-22.0	-43.0	2337
	-20.3	-44.7	2328
	-18.5	-46.5	2329
	-16.8	-48.2	2322
	-15.0	-50.0	2308
	-13.3	-51.7	2308
	-11.6	-53.4	2295
	-9.8	-55.2	2294
[SII] 6730	-61.7	-3.2	2431
	-60.0	-5.0	2406
	-47.4	-17.6	2424
	-45.6	-19.4	2424
	-43.9	-21.1	2431
	-42.1	-22.9	2408
	-40.4	-24.6	2405
	-38.6	-26.4	2386
	-36.9	-28.1	2386
	-29.9	-35.1	2368
	-22.9	-42.1	2315
	-21.2	-43.8	2325
	-19.4	-45.6	2328
	-17.7	-47.3	2326
	-15.9	-49.1	2315
	-14.2	-50.8	2312
	-12.4	-52.6	2306
	-10.7	-54.3	2291

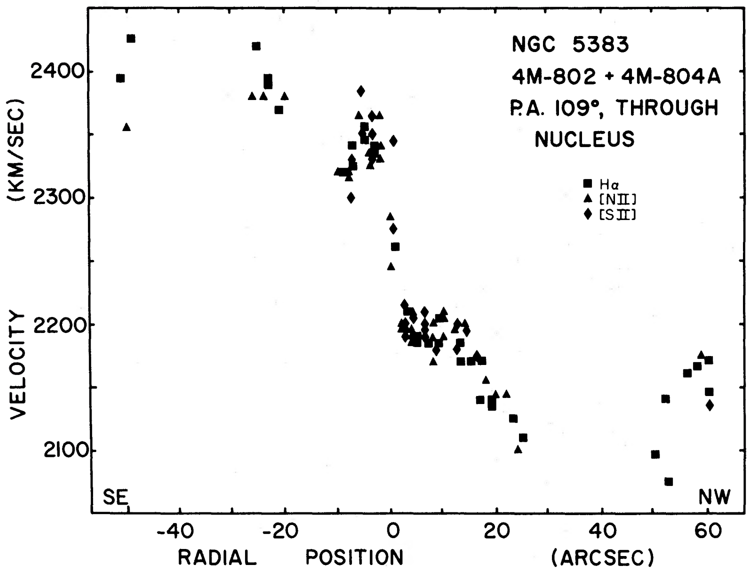

FIG. 4*a*.—Observed line-of-sight velocities (heliocentric) along position angle 109° through the nucleus (position 9), showing the complex velocity pattern across NGC 5383.

be an overestimate of the hydrogen mass for NGC 5383 caused by the presence of NGC 5383a in the beam. If we make the assumption that the NGC 5383 profile is symmetrical, then approximately 10% of the signal comes from hydrogen in the companion. The mass of hydrogen in NGC 5383 is then $9 \times 10^9 \mathscr{M}_\odot$, in excellent agreement with preliminary data from Westerbork (Allen *et al.* 1974, converted to our distance), which yields $9.1 \times 10^9 \mathscr{M}_\odot$. The distance-independent ratio of hydrogen mass to optical luminosity is 0.23. The mass of the companion is then $9 \times 10^8 \mathscr{M}_\odot$, a value which is in general accord with the hydrogen masses seen in the dwarf galaxies surveyed by Fisher and Tully (1975). It is likely, however, that the assumption of a symmetrical profile for NGC 5383 is an oversimplification. As we discuss below, the velocity field for NGC 5383 shows large-scale deviations from circular rotation, and hence the 21 cm profile could be asymmetrical.

The half-width of the observed velocity profile

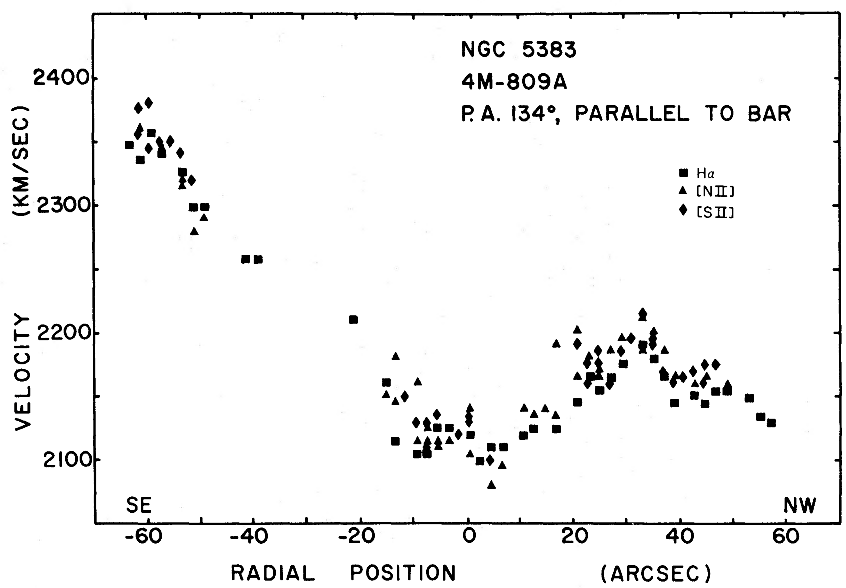

FIG. 4*b*.—Observed line-of-sight velocities (heliocentric) along position angle 134°, parallel to the bar, but offset 7″ southwest to go through emission knots (position 11). The position angle of this spectrum is the closest match for the position angle of the data illustrated in Fig. 3 of Burbidge *et al.* 1962. Both sets of data are in overall agreement in showing the asymmetry of the rotation curve along the bar.

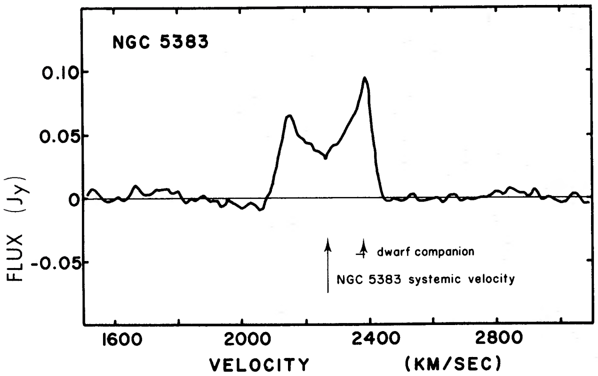

FIG. 5.—The 21 cm neutral-hydrogen velocity profile for NGC 5383, from observations with the NRAO 91.4 m telescope. The long arrow marks the centroid of the profile at 2264 ± 6 km s^{-1}. The short arrow is at the mean optical velocity of the dwarf companion; the cross bar gives the range of hydrogen velocities seen by Westerbork observers (Sancisi 1976*a*) in the companion.

(read at 20% of the peak value on the low-velocity side) is $\Delta V/2 = 166 \pm 4$ km s^{-1}, and the centroid is $V = 2264 \pm 6$ km s^{-1}. From the Westerbork observations, $\Delta V/2 = 174$ km s^{-1}, and $V = 2250 \pm 15$ km s^{-1}. Neutral hydrogen at the position of the companion is seen in the Westerbork mapping (Sancisi 1976*a*) in the velocity range 2360–2380 km s^{-1}, which compares well with our optical value $V = 2379 \pm 25$ km s^{-1} and a total observed optical velocity spread of 30 km s^{-1} along P.A. 156°. The dynamical mass is $\mathscr{M}_{21} = 1.7 \times 10^{-2} D_{\rm pc}\, d' (\Delta V/2 \sin i)^2$ (Roberts 1962), where D is the galaxy distance in pc, and d is the diameter in arcmin. For NGC 5383, $\mathscr{M}_{21} = 2.0 \times 10^{11} \mathscr{M}_\odot$. We discuss this value in § V.

III. THE VELOCITY FIELD OF NGC 5383

In order to analyze the velocity field of NGC 5383, it is necessary to know the systemic velocity of the galaxy, the orientation of the galaxy in space, i.e., the position angle on the sky of the line of nodes, the angle of inclination, and which side of the galaxy is the nearer side. Six of our spectra pass through the nucleus; the four 4 m plates give $V = 2264 \pm 5$ km s^{-1} (heliocentric), which we adopt as the systemic velocity. This is in excellent agreement with $V = 2264$ (Burbidge, Burbidge, and Prendergast 1962); with the NRAO 21 cm result, $V = 2264 \pm 6$ km s^{-1}; and with the Westerbork results, $V = 2250 \pm 15$ km s^{-1} (Allen *et al.* 1974). It agrees poorly with the value of Cheriguene (1975) of $V = 2220$ km s^{-1}.

The velocity field of NGC 5383, after removal of the systemic velocity, is shown in Figure 6*a*. It is clearly complex and cannot be interpreted in terms of circular velocities only. The linear velocity gradients across the nucleus can be used to determine a kinematical line of nodes, assuming only circular velocities (Burbidge and Burbidge 1960). From our observations in four position angles, we calculate $\phi = 78° \pm 4°$; this is marked on the velocity field in Figure 6*a*. It is in poor agreement with the line of nodes ($\phi = 50°$) which might be chosen from inspection of the overall velocity field, i.e., the line perpendicular to the iso-velocity curves immediately outside the nuclear region (Fig. 6*b*).

Alternatively, if the assumption is made that the galaxy is circular in its principal plane, the position angle of the line of nodes and the inclination may be found from the ellipse formed by the projection of the galaxy onto the plane of the sky. In this manner, Burbidge, Burbidge, and Prendergast (1962) find $\phi = 94°$, and Nilson (1973) gives $\phi = 85°$. There is no agreement between the kinematical line of nodes, determined either from the nuclear velocity gradients or from the overall velocity pattern, with this morphological line of nodes. This is not too surprising; a recurrent problem in the study of barred spiral galaxies has been the understanding of the true spatial structure of these objects (Rubin, Thonnard, and Ford 1975). Most likely the assumption that the galaxy is circular in its principal plane is incorrect.

From the axial ratio of the optical image of NGC 5383, an inclination of 40° is determined (Burbidge, Burbidge, and Prendergast 1962; de Vaucouleurs and de Vaucouleurs 1964). However, we show below that, if the plane of NGC 5383 is warped, the inclination ranges from 20° at small nuclear distance to 55° at large distance.

The pattern of dust lanes does not conclusively indicate which side of the galaxy is nearest to the observer. Burbidge, Burbidge, and Prendergast (1962) implicitly assumed that the north side of the galaxy is the near side. However, we adopt the convention of trailing spiral arms, so that *the south or southeast side of NGC 5383 is the near side*. This assumption is critical to all models which follow.

IV. INTERPRETATION OF THE VELOCITY FIELD

Because the velocity field of NGC 5383 does not fit the pattern for circular rotation, a variety of other models have been considered. We first discuss the velocity gradients across the nucleus. Next we consider the large-scale velocity field in the galaxy, in terms of a model with streaming motions superposed on a rotation. We use the observed velocities at large distances (spiral arm region) to define the rotation curve and orientation of the line of nodes. The residual velocities are then attributed to non-circular motions associated with the dynamics of the bar.

Alternatively, if the kinematics of NGC 5383 have been disturbed by gravitational interaction with the companion, the less-dense outermost regions would be most affected. The second model uses the inner velocities to define the circular rotation and studies the irregularities in the outer regions.

A third model considers whether a simple symmetrical warp on the plane of the galaxy can explain the observed velocity field.

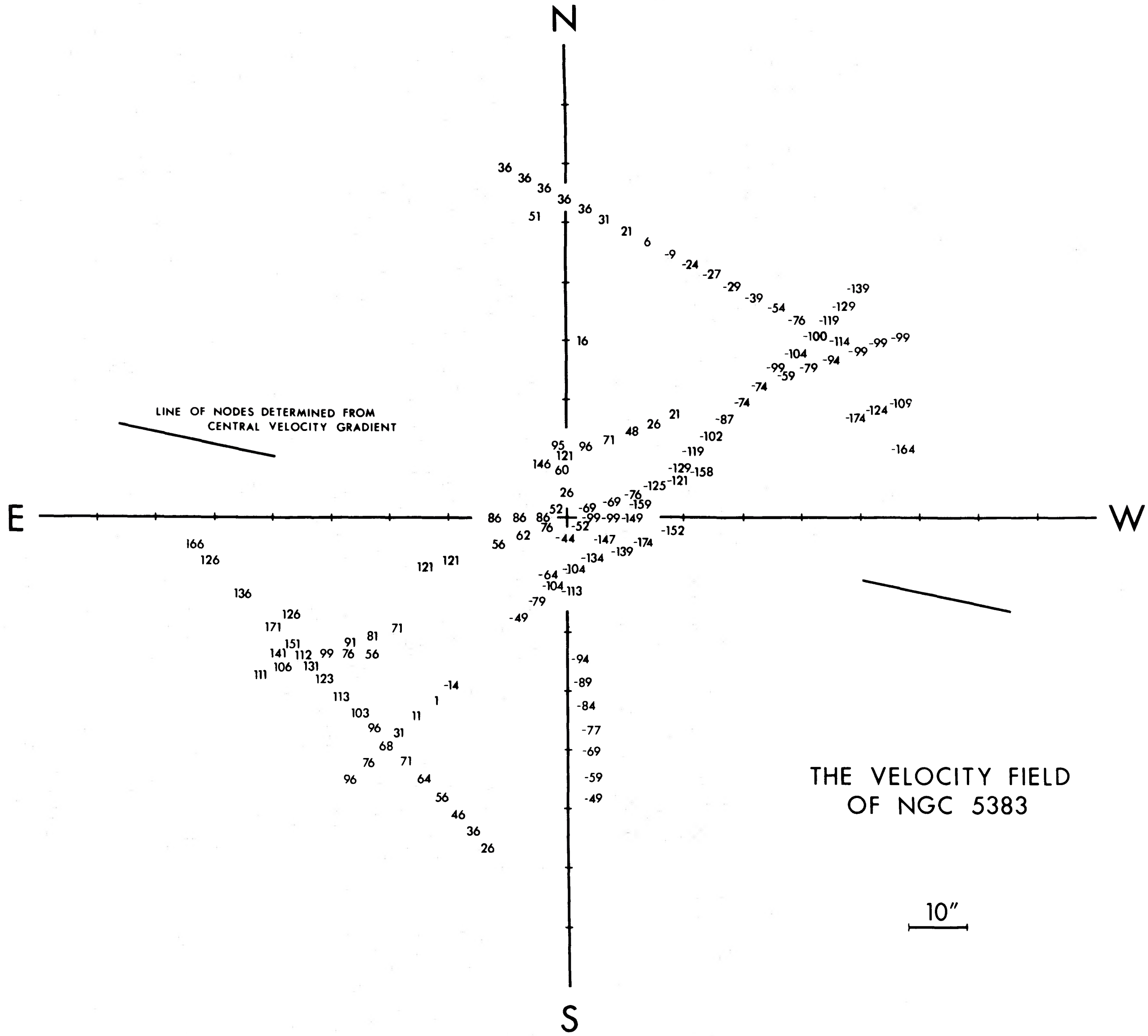

FIG. 6*a*.—The velocity of the barred spiral galaxy NGC 5383, with respect to the systemic velocity of 2264 km s^{-1}. Note large gradient in velocity across the bar.

a) *Noncircular Motions near the Nucleus*

We assume linear gradients for both the rotation $V(R)$ and expansion $E(R)$ velocities of the nuclear gas; then

$$\frac{dV}{ds}(s, \eta) = \frac{dV(R)}{dR} \sin i \cos (\eta - \phi)$$

$$- \frac{dE(R)}{dR} \tan i \sin (\eta - \phi) ,$$

where (dV/ds) is the observed velocity gradient in position angle η on the plane of the sky, R is the distance from the nucleus, and i and ϕ are the inclination and position angle of the line of nodes. From the observed velocity gradients in the nucleus, and an analysis following that described elsewhere (Rubin, Ford, and Peterson 1975), the following pattern of velocities results:

1. If only circular motions are present in the nucleus, then $\phi = 78°$ and $V(R) = 158 \pm 7$ km s^{-1} at the edge of the 3″.5 = 800 pc linear gradient region in the nucleus. We show below that $\phi = 70°$ for the nucleus on a warped-disk model; hence purely circular motions in the nucleus exist in the warped model.

2. If $\phi = 50°$, as deduced from the overall large-

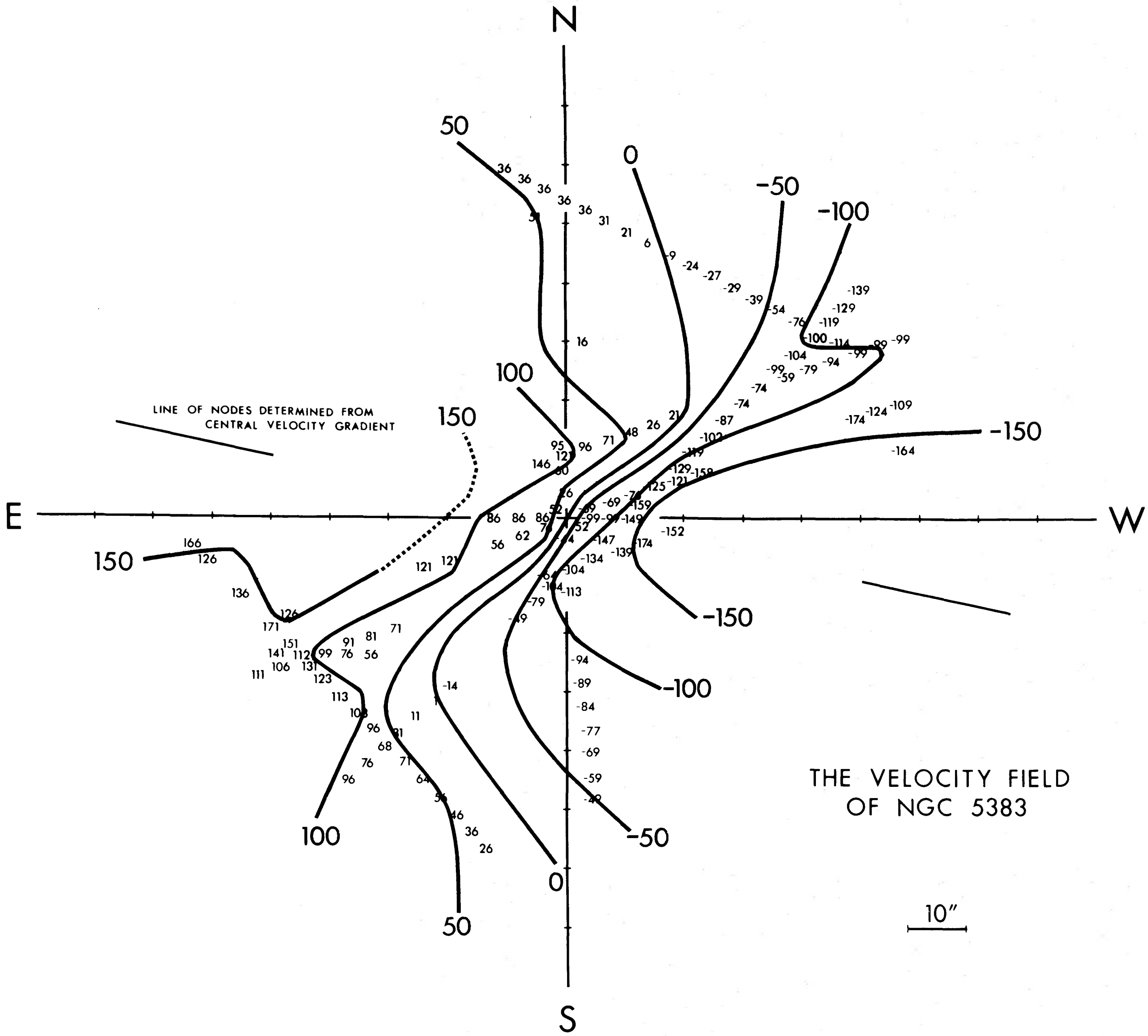

FIG. 6*b*.—The same as Fig. 6*a*, but with isovelocity contours drawn (eye estimates)

scale velocity pattern, then there is a contraction with $E(R) = -60 \pm 10$ km s^{-1} and $V(R) = 136 \pm 10$ km s^{-1} at $R = 800$ pc. A rotating nucleus with no radial motions is a poor fit to the observations if $\phi = 50°$.

3. If $\phi = 90°$ on the basis of the geometry of the outer isophotes, then $V(R) = 154 \pm 10$ km s^{-1} at $R = 800$ pc, with a barely significant expansion $E(R) = 24 \pm 10$ km s^{-1}. We have shown elsewhere (Rubin, Thonnard, and Ford 1975), in a study of NGC 6764, another barred spiral, that the assumption of circular arms is difficult to support in S-type barred spirals; we consider case 3 least likely.

The possibility that rotation and contraction velocities exist in the gas near the nucleus of NGC 5383 cannot be ruled out (case 2). In NGC 3351, a previously studied barred spiral galaxy (Rubin, Ford, and Peterson 1975), contraction and rotation motions are clearly seen in the nuclear region, $r < 300$ pc.

Duus and Freeman (1975) have suggested a theoretical explanation which can account for the origin of the structure of the nuclear region of NGC 5383. Of the test particles in the potential field of a galactic disk plus a rotating bar, two-thirds fell to the center of the bar. Here they form a persistent two-clump structure whose orbital period about the center differs considerably from the rotational period of the bar; the mean velocities of the two clumps relative to the bar are of the order of 50–100 km s^{-1}. The optical nuclear structure may thus be a direct consequence of the existence of the bar.

b) *Streaming Motions in a Planar Disk due to the Presence of a Bar*

Are there streaming motions in the gas in NGC 5383 which can be attributed to the dynamical effect of the bar? We examine the velocity field under two simplifying assumptions (following van der Kruit 1976):

1. The galaxy is a plane. Although warping of galactic disks is not an uncommon phenomenon, most evidence suggests that disks of galaxies are disturbed only in regions where the mass density is very small, generally beyond the optical image (see, for example, Sancisi 1976*b*).

2. The velocities are part of a large-scale pattern of streaming, which is a perturbation caused by the bar superposed upon the normal rotation of the disk. The tangential and radial components of the streaming are subject to several physical constraints. (*a*) There is a deceleration of the radial motion with radius if the streaming is outward (acceleration if inward). (*b*) The tangential motions are consistent with the conservation of angular momentum. (*c*) There are no z-direction motions, consistent with the first assumption that the galaxy is a planar disk.

For several forms of the rotation curve, and for a range of inclinations, the predicted line-of-sight velocity field on the plane of the sky was computed. In Figure 7 we show an example of a velocity field due to a rotation onto which are superposed the line-of-sight residuals due to noncircular motions. For this model, $\phi = 82°$, a compromise which minimizes the residuals in the two arms.

This model, which is of course not unique, produces residual velocities in the bar which are generally *outward*. Within 20″ of the nucleus, the observed residuals are 100 km s^{-1}, corresponding to 180 km s^{-1} in the plane of the galaxy; near the ends of the bar, the outward velocities are $\sim$70 km s^{-1} in the plane of the galaxy. The deviations are not significantly smaller if tangential motions or z motions are permitted, or if a different geometry is adopted.

The velocity residuals in the arms are small, but nonzero. With respect to the nucleus, the NW arm is moving outward and the SE inward, which is an unlikely circumstance.

In summary, a pattern of high-velocity gas streaming outward along the bar of a planar galaxy can account for the observations, although residual velocities exist in the arms.

c) *Streaming Motions in the Spiral Arm Regions*

A model in which the velocity residuals are minimized in the central regions is shown in Figure 8. This requires a rotation curve with an unacceptable high $V_{\max} \sim$ 500 km s^{-1}. The large remaining residuals are in the sense that the arms are moving inward. We do not consider this an acceptable model.

d) *A Warped-Disk Model*

We have shown that any model which restricts the geometry of NGC 5383 to a plane requires the presence of large noncircular motions. We now explore the possibility that the complex observed pattern of velocities in NGC 5383 is due to a warp in the plane of the galaxy. In NGC 5383 the zero velocity contour is not a straight line which defines a kinematical minor axis; it forms an S-shape across the galaxy, bending eastward in the NW quadrant of the galaxy, and bending westward in the SE quadrant (Fig. 6*b*). A similar distortion is seen in the velocity contours for ± 50 and ± 100 km s^{-1}. S-shaped isovelocity contours in a galaxy are a good indicator of a warped disk. This distorted velocity pattern is very similar to that observed in high-spatial-resolution 21 cm observations of M83 (Rogstad, Lockhart, and Wright 1974), a spiral galaxy whose morphology shows some similarity to an open bar structure like NGC 5383, and whose ragged outer structure is similar to that seen in Figure 2*a*. These authors were able to reproduce the observed velocity field and the projected surface density in neutral hydrogen in M83 by use of a warped-disk model in which the inclination varies smoothly from 20° over the optical image to 50° or 60° at large radii, and the major axis position angle rotates from 45° to 115°.

We have adopted their model for M83 to compare with the kinematic data of NGC 5383 (Fig. 9), rather than deriving a new model. The variations adopted for $V(R)$, $i(R)$, and $\phi(R)$ are shown in Figure 9. The rotation velocities rise to 300 km s^{-1} at about 5 kpc, and decrease only slightly out to R = 20 kpc. The inclination of the plane of the galaxy to the plane of the sky is only $\sim$20° for small R, increases to $<$40° at the end of the bar, and becomes more nearly edge-on ($i \approx 55°$) for large R. The major axis of the galaxy rotates with increasing R, from +70° to −50°. As can be seen in Figure 9, the distortion of the isovelocity contours along the bar is not so severe as to make the model unacceptable. Along the bar are generally small streaming motions; toward the nucleus on the far side, away from the nucleus on the near side. For NGC 5383 the largest residuals from this model are smaller than those in either of the planar-disk models discussed above. Additional modifications would most likely reduce the residuals even more, but we have not attempted such a refinement. The assumption of a warped disk in NGC 5383 gives the best fit to the observed velocities of any of the models which we have considered. The presence of a companion at a projected distance of only 45 kpc offers a possible explanation for such a bending of the principal plane.

With the adopted rotation curve for NGC 5383 (Fig. 9), a mass of $\mathscr{M}_{\text{opt}} = 2.4 \times 10^{11}\ \mathscr{M}_\odot$ is calculated out to r = 20 kpc.

The optical velocities reported in this paper are consistent with the two models discussed above: a rotating warped disk, or a rotating planar disk with outward-streaming motions in the bar. We anticipate that the combination of the detailed optical observations, $R < 60''$, with the more extended Westerbork 21 cm line velocities, $R > 60''$, will be necessary to reveal the true structure and dynamics of NGC 5383. Preliminary Westerbork results made available after the submission of this paper (Sancisi 1977) show a

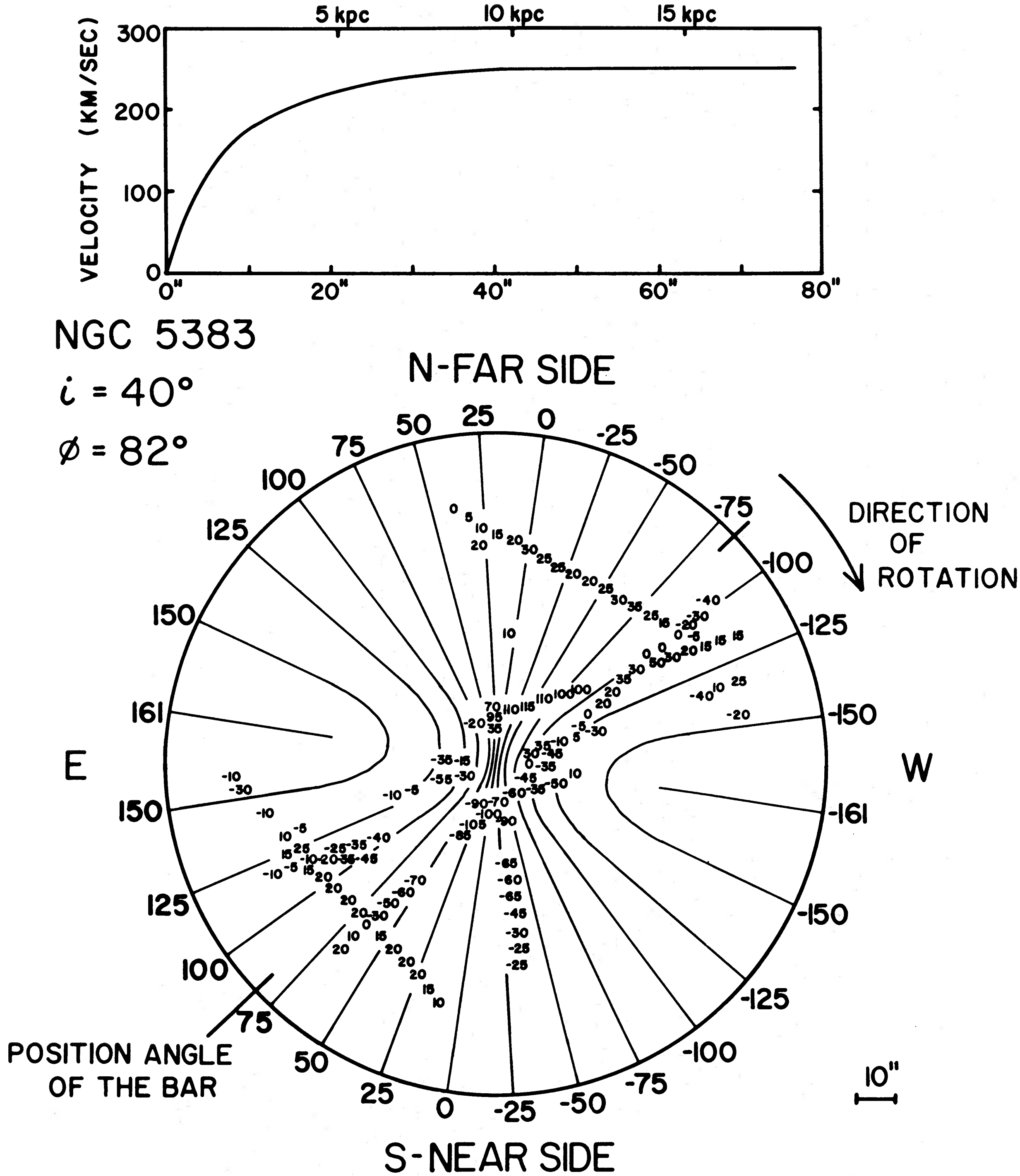

FIG. 7.—Planar-disk model for the velocity field of NGC 5383, chosen to minimize velocity residuals in the spiral arm region. *Top*, model rotation curve. *Bottom*, the grid of solid lines represents the line-of-sight velocity field on the plane of the sky for the rotation curve above; $i = 40°$, and $\phi = 82°$ are assumed. The velocities in km s^{-1} are indicated around the circle. The residual velocities, $\Delta V = V_{\text{observed}} - V_{\text{model}}$, rounded to the nearest 5 km s^{-1}, are superposed on the grid and represent the line-of-sight component of the noncircular velocity field. The position angle of the bar is indicated. Note large positive residuals (*far side*) and negative residuals (*near side*) which are interpreted as outward-streaming motions.

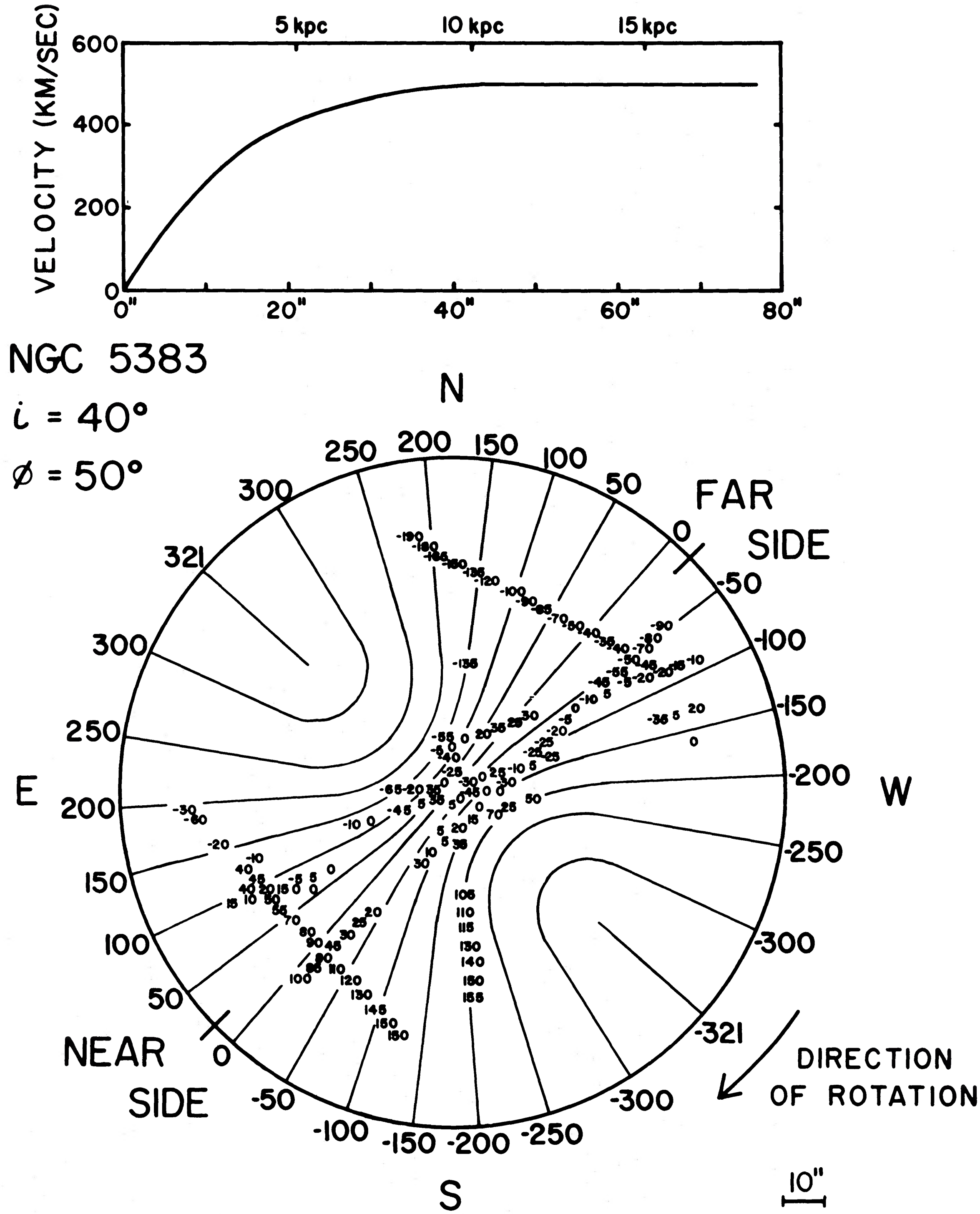

FIG. 8.—Planar-disk model for the velocity field of NGC 5383, chosen to minimize the residuals over the inner regions of the galaxy. *Top*, the adopted rotation curve. *Bottom*, the grid of solid lines represents the line-of-sight velocity field on the plane of the sky for the adopted rotation curve; $i = 40°$ and $\phi = 50°$. The residual velocities, $\Delta V = V_{\text{observed}} - V_{\text{model}}$, are shown superposed on the grid.

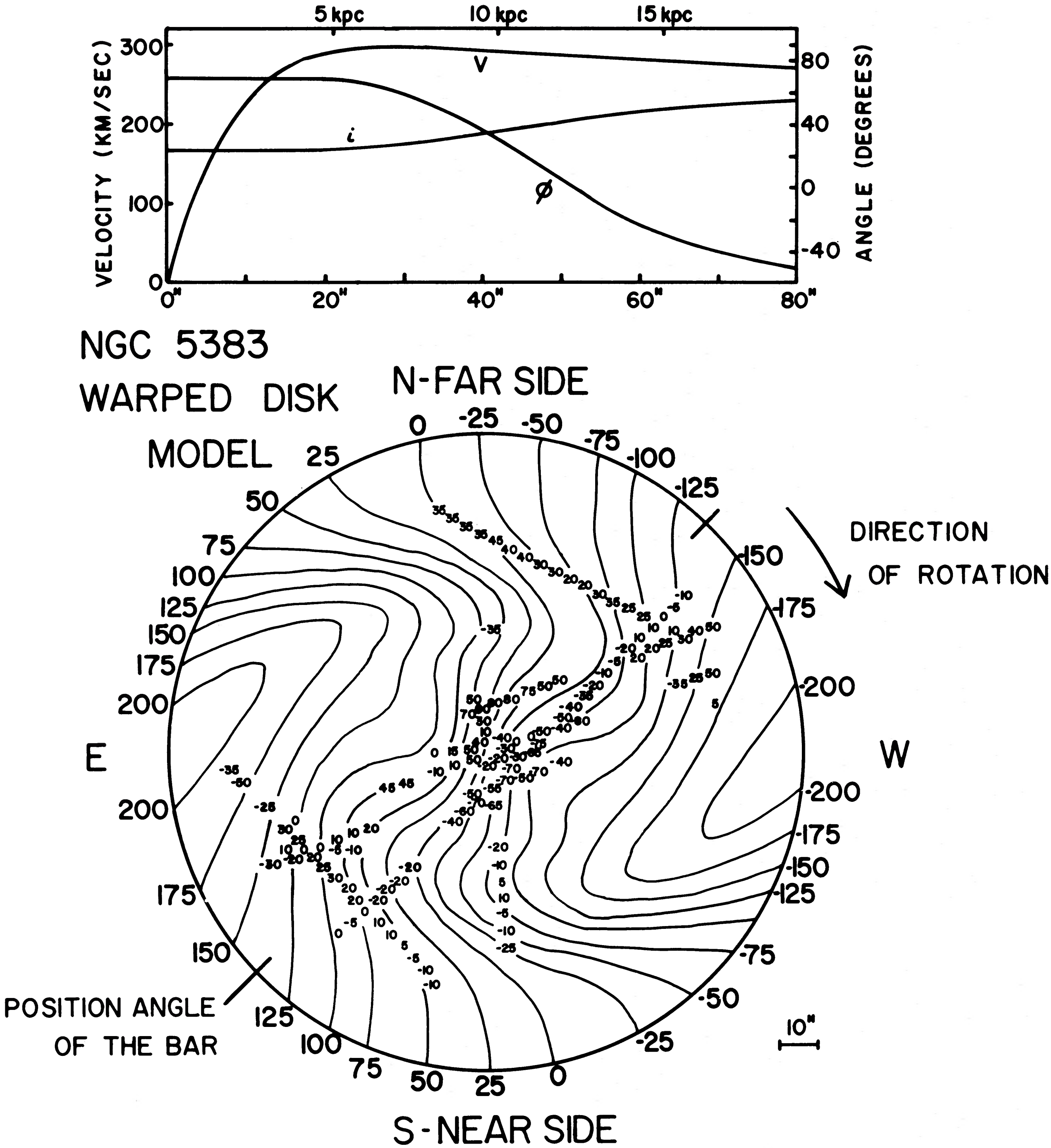

FIG. 9.—A symmetrical warped-disk model for the velocity field of NGC 5383. *Top*, the rotation curve, variation of inclination i, and the position angle ϕ of the line of nodes as a function of radius, adapted from Rogstad *et al.* 1974. *Bottom*, the grid of solid lines represents the line-of-sight velocity field on the plane of the sky. The velocities in km s^{-1} are indicated around the circle. The residual velocities, $\Delta V = V_{\text{observed}} - V_{\text{model}}$, rounded to the nearest 5 km s^{-1}, are shown superposed on the velocity grid. The model grid has been oriented to minimize the residual velocities over the entire galaxy.

TABLE 3
PARAMETERS FOR NGC 5383 AND NGC 3351

Parameter	NGC 5383	NGC 5383a	NGC 3351
V_0 (km s^{-1})	2365	2480	645*
Distance (Mpc)	50	50	10*
b	+70	+70	+56
m_{Hc} (de Vaucouleurs *et al.* 1976)	12.18	...	10.73
m (Nilson 1973)	12.5	16.5:	11.2
Diameter (Nilson 1973)	3′.5:	1′.3	8′.5
Diameter (kpc)	51	19	25
i (degrees)	$\sim$20, r = 0″, $\sim$55, r = 80″	...	40*
$(B - V)$ (de Vaucouleurs *et al.* 1976)	0.72	...	0.83
$(U - B)$ (de Vaucouleurs *et al.* 1976)	0.07	...	0.25
r of most distant velocity	16 kpc	...	200″ = 9.7 kpc*
M_B	−21.3	−17.0:	−19.27
L_B ($L_\odot$)	4.8×10^{10}	$\sim 9 \times 10^8$	7.4×10^9
H I flux (Jy)	16.7 ± 2		72 ± 14*
$\Delta V/2$ (21 cm; km s^{-1})	166	...	141*
$V_{max} = (\Delta V/2 \sin)$ (km s^{-1})	$\sim$260	...	220*
$\mathcal{M}_{\text{H I}}$ ($\mathcal{M}_\odot$)	9×10^9	$\sim 9 \times 10^8$	1.7×10^9
$\mathcal{M}$(21 cm profile) ($\mathcal{M}_\odot$)	2.0×10^{11}	...	7×10^{10}
$\mathcal{M}_{\text{H I}}/\mathcal{M}_{21}$	0.045	...	0.024
$\mathcal{M}_{\text{H I}}/L$ ($\mathcal{M}_\odot L_\odot^{-1}$)	0.19	...	0.23
$\mathcal{M}$(rot. curve) ($\mathcal{M}_\odot$)	2.4×10^{11} (d = 40 kpc)	...	6×10^{10} (d = 19 kpc)
$\mathcal{M}/L$ ($\mathcal{M}_\odot L_\odot^{-1}$)	5	...	8
$\mathcal{M}VR$ ($\mathcal{M}_\odot$ km s^{-1} kpc^{-1})	9×10^{14} (d = 40 kpc)	...	9×10^{13} (d = 19 kpc)

* Peterson *et al.* 1976.

nondistorted velocity field at large nuclear distances and may favor a planar model.

V. A COMPARISON OF THE BARRED SPIRAL GALAXIES NGC 5383 AND NGC 3351

Optical velocities and 21 cm observations are now available from our observations for the two barred spiral galaxies, NGC 5383 and NGC 3351 (Peterson *et al.* 1976). Some of their parameters are compiled in Table 3 and discussed below. Because it is nearer, NGC 3351 is apparently brighter and of larger angular diameter. However, NGC 5383 is 2 mag intrinsically brighter and twice as large. The distance-independent ratio of hydrogen mass to optical luminosity is $\sim$0.2 for both. For NGC 5383, the dynamical mass calculated from the width of the velocity profile and a diameter of 51 kpc is $\mathcal{M}$(21 cm profile) = 2.0×10^{11} $\mathcal{M}_\odot$, which agrees reasonably well with the mass deduced from the rotation curve out to a diameter of 40 kpc, $\mathcal{M}$(rot. curve) = 2.4×10^{11} $\mathcal{M}_\odot$. For NGC 3351 also, the 21 cm and optical masses are in good agreement: $\mathcal{M}$(21 cm profile) = 7×10^{10} $\mathcal{M}_\odot$ (diam. = 25 kpc), and $\mathcal{M}$(rot. curve) = 6×10^{10} $\mathcal{M}_\odot$ (diam. = 19 kpc).

For NGC 5383, 5% of the total mass is neutral hydrogen, and the mass-to-blue-luminosity ratio is about 5. For NGC 3551, comparable numbers are $2\frac{1}{2}$% H I and $M/L_B = 8$. The $U - B$ and $B - V$ colors for both galaxies, corrected for redshift, inclination, and galactic latitude, are reasonably similar; NGC 5383 is slightly bluer. This bluer color is consistent with the higher hydrogen mass (Roberts 1975), but these two galaxies do not exhibit the higher M/L_B ratios with increasing luminosity found for elliptical galaxies (Faber and Jackson 1976).

For NGC 3351 and NGC 5383, the angular momenta are $H = 9 \times 10^{13}$ $\mathcal{M}_\odot$ kpc km s^{-1} and $H = 9 \times 10^{14}$ $\mathcal{M}_\odot$ kpc km s^{-1}, respectively; these are within the range for nonbarred spirals (Nordsieck 1973) and do not support the conjecture that barred spirals have higher values of H.

VI. CONCLUSIONS

The emission-line velocity field of NGC 5383 does not resemble that expected for a pattern of circular motions only. The velocities in the bar and the spiral arm region can be most closely reproduced by a simple rotation in a disk which is substantially warped. The distortion could have arisen from a recent encounter with the dwarf spiral companion of low surface brightness which lies only 45 kpc (projected distance) south of NGC 5383.

Velocities of the excited gas in the nucleus exhibit a simple sinusoidal dependence on position angle, but a unique interpretation requires knowledge of the geometry of the galaxy. For the warped-disk model, $\phi = 70°$, and only rotational velocities are present in the nucleus. With this interpretation there are no major problems in understanding the observed velocity field of NGC 5383.

An alternative planar model indicates both rotation and large outward-streaming motions in the bar, and rotation plus contraction motions in the nucleus, but in general the pattern of circulation predicted by theory is not observed. It is worth recalling that NGC 3351, a Θ type barred spiral, which we have previously studied (Rubin, Ford, and Peterson 1975), has a well-defined geometry and a simple pattern of rotation both in the stars and in the gas outside of the nucleus. With the exception of contraction motions in the nucleus of NGC 3351, the presence of a fairly prominent bar has not distorted the velocity pattern from that of a normal nonbarred spiral. In NGC 5383, we have no information concerning the stellar velocity field. For the gas, a normal pattern of rotation, coupled with either a warped disk or a planar disk with large outward-streaming motions, can reproduce the observations. Whether this is evidence of significant large-scale dynamical differences between barred and nonbarred spiral galaxies must still be established. In both galaxies, the 21 cm integrated H I profiles are typical of conventional nonbarred spirals; these galaxies could not be identified as barred spirals by their integrated 21 cm neutral-velocity hydrogen distribution.

We would like to thank Drs. R. Sancisi and W. T. Sullivan for information and discussion of NGC 5383 prior to publication of the results of the Westerbork studies. We thank Dr. L. Goldberg for observing time at KPNO, Dr. D. Heeschen for observing time at NRAO, and Dr. J. Hall for observing time at Lowell Observatory.

REFERENCES

Allen, R. J., Goss, W. M., Sancisi, R., Sullivan, W. T., and van Woerden, H. 1974, in *IAU Symposium No. 58, Formation and Dynamics of Galaxies*, ed. J. R. Shakeshaft (Dordrecht: Reidel), p. 425.
Burbidge, E. M., and Burbidge, G. R. 1960, *Ap. J.*, **132**, 30.
Burbidge, E. M., Burbidge, G. R., and Prendergast, K. H. 1962, *Ap. J.*, **136**, 704.
Cheriguene, M. F. 1975, in *La Dynamique des Galaxies*, ed. L. Weliachew (Paris: CNRS), p. 439.
de Vaucouleurs, G., and de Vaucouleurs, A. 1964, *Reference Catalogue of Bright Galaxies* (Austin: University of Texas Press).
de Vaucouleurs, G., de Vaucouleurs, A., and Corwin, H. G. 1976, *Second Reference Catalogue of Bright Galaxies* (Austin: University of Texas Press).
Duus, A., and Freeman, K. C. 1975, in *La Dynamique des Galaxies*, ed. L. Weliachew (Paris: CNRS), p. 419.
Faber, S. M., and Jackson, R. E. 1976, *Ap. J.*, **204**, 668.
Fisher, J. R., and Tully, R. B. 1975, *Astr. Ap.*, **44**, 151.
Lynds, B. T. 1972, in *External Galaxies and Quasi-Stellar Objects*, ed. D. S. Evans (Dordrecht: Reidel), p. 56.
———. 1974, *Ap. J. Suppl.*, **28**, 391.
Nilson, P. 1973, "Uppsala General Catalogue of Galaxies," *Uppsala Astr. Obs. Ann.*, Ser. V: A., Vol **1**.
Nordsieck, K. H. 1973, *Ap. J.*, **184**, 734.
Pease, F. G. 1917, *Ap. J.*, **46**, 24.
Peterson, C. J., Rubin, V. C., Ford, W. K., Jr., and Thonnard, N. 1976, *Ap. J.*, **208**, 662.
Roberts, M. S. 1962, *A.J.*, **67**, 437.
———. 1975, in *Galaxies and the Universe*, ed. A. Sandage, M. Sandage, and J. Kristian (Chicago: University of Chicago Press), p. 309.
Rogstad, D. H., Lockhart, I. A., and Wright, M. C. H. 1974, *Ap. J.*, **193**, 309.
Rubin, V. C., Ford, W. K., Jr., and Peterson, C. J. 1975, *Ap. J.*, **199**, 39.
Rubin, V. C., Thonnard, N., and Ford, W. K., Jr. 1975, *Ap. J.*, **199**, 31.
Sancisi, R. 1976*a*, private communication.
———. 1976*b*, *Astr. Ap.*, **53**, 159.
———. 1977, private communication.
Sandage, A. R. 1961, *The Hubble Atlas of Galaxies*, Carnegie Institution of Washington Publication No. 618.
van der Kruit, P. C. 1976, *Astr. Ap.*, **49**, 161.

W. Kent Ford, Jr., Vera C. Rubin, and Norbert Thonnard: Department of Terrestrial Magnetism, Carnegie Institution of Washington, 5241 Broad Branch Road, NW, Washington, DC 20015

Charles J. Peterson: Cerro Tololo Inter-American Observatory, Casilla 63-D, La Serena, Chile

1978ApJ...219...31P

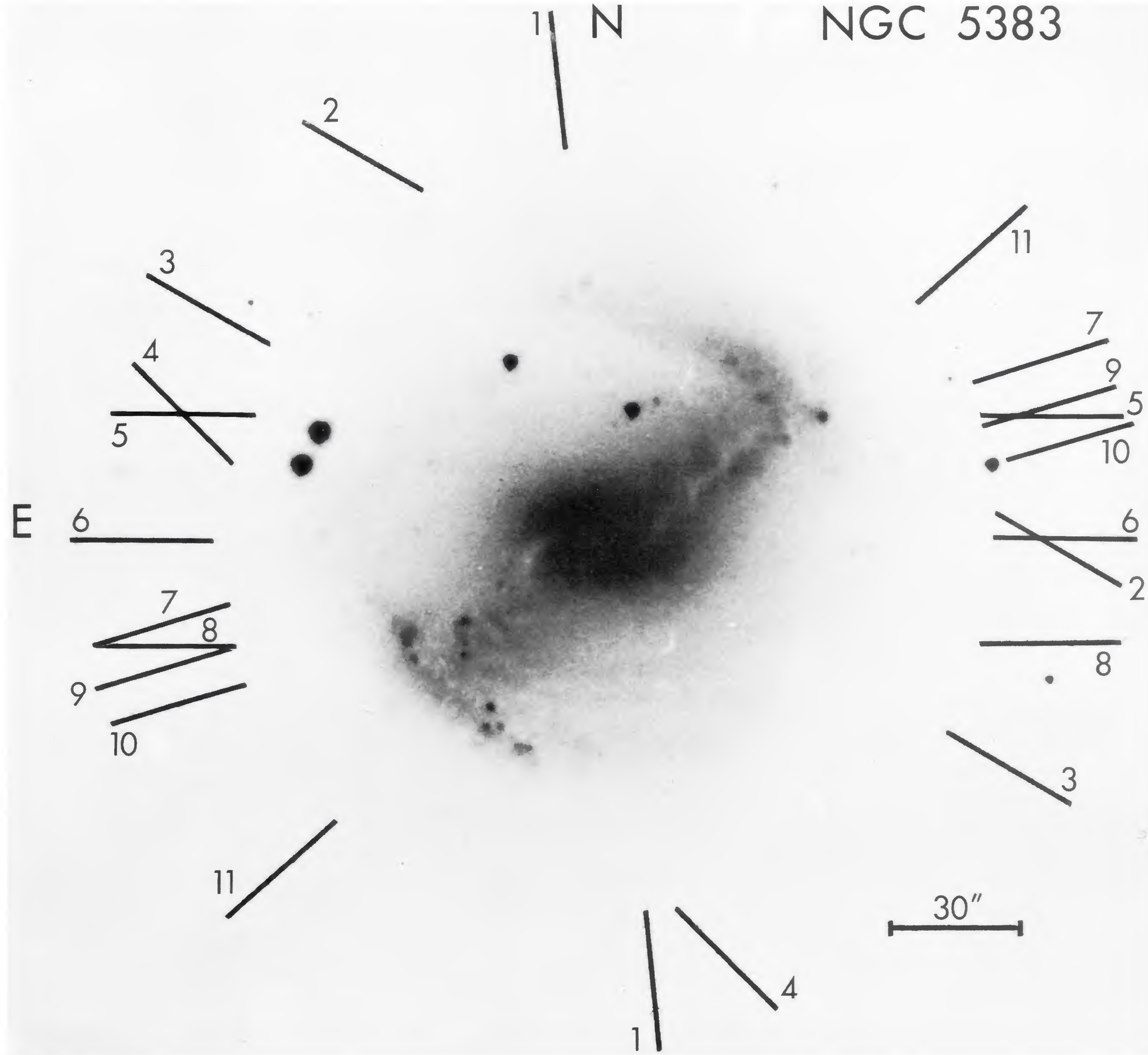

FIG. 1.—NGC 5383, showing the positions of the spectrograph slit for the spectra listed in Table 1. Plate 4M-116, 12 minute Cassegrain exposure at the 4 m Mayall telescope on a N_2-baked IIIa-J plate using a Carnegie image tube plus RG2 filter (effective wavelength in the red).

PETERSON *et al.* (*see* page 31)

1978ApJ...219...31P

PLATE 2

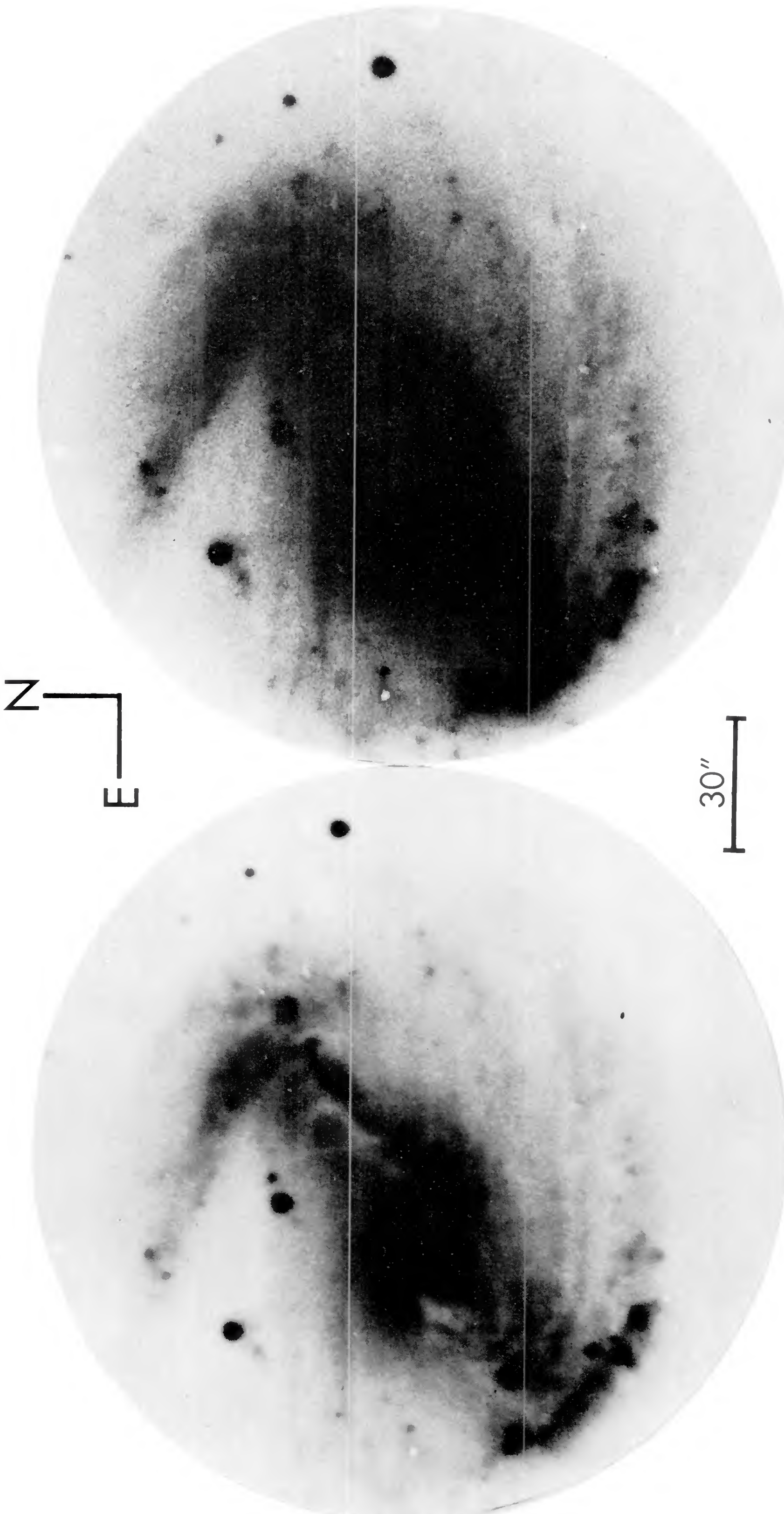

FIG. 2*a*.—Two prints from the same plate (4M-96, 12 minute exposure, N_2-baked IIIa-J plate plus Carnegie image tube plus 4 m telescope plus 5030 filter) to illustrate the structure of the absorption features (*left*) and the structure of the outer spiral arm region (*right*).

PETERSON *et al.* (*see* page 31)

NGC 5383 AND COMPANION

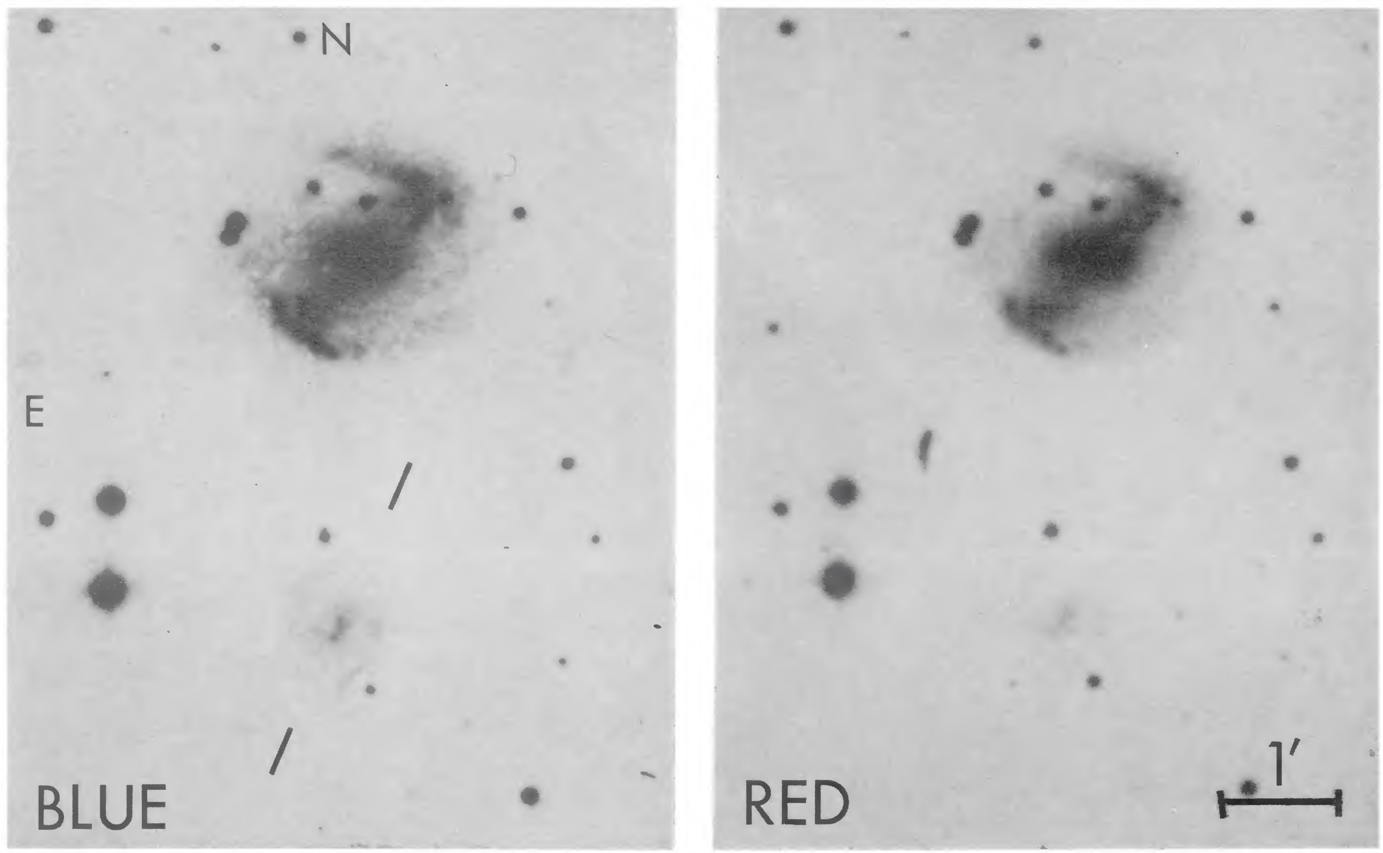

FIG. 2*b*.—NGC 5383 and its low-surface-brightness companion to the south, separation on the sky = 3′; reproduced from the blue and red copies of the Palomar Sky Survey prints. The two short dashes on the blue photograph indicate the position of the slit (P.A. 156°) for the spectrum of the companion galaxy. Reproduction courtesy of Hale Observatories.

PETERSON *et al.* (*see* page 31)

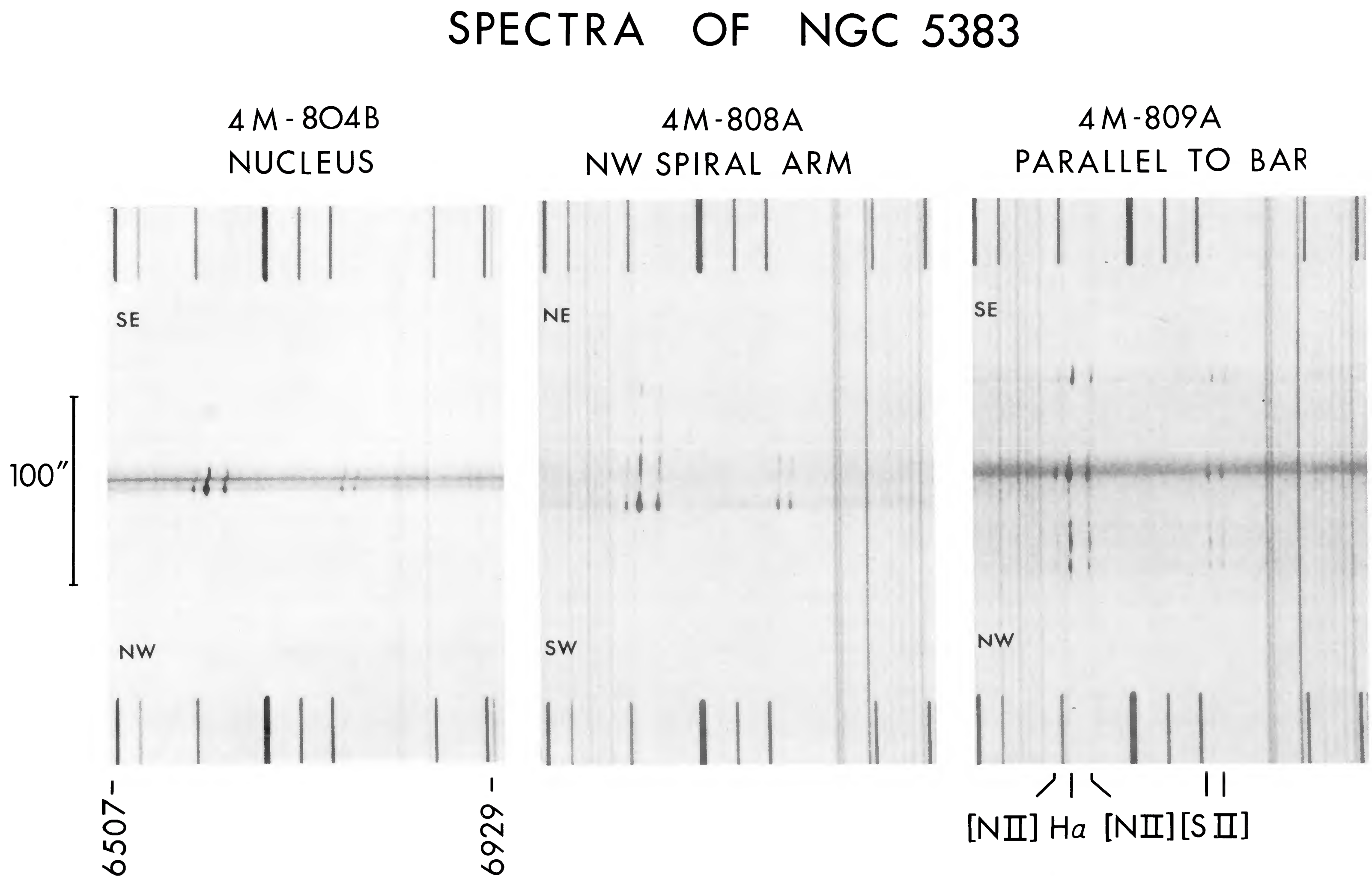

FIG. 3a.—Representative spectra of NGC 5383, showing the emission lines of Hα, [N II], and [S II] in the red. From left to right, the spectra are 4M-804B (position angle 109° through nucleus), 4M-808A (position 2 passing through the northeast spiral arm), and 4M-809A (position 11 parallel to the axis of the bar). Exposure time, respectively, of 60, 107, and 85 minutes, N_2-baked IIIa-J plates plus Carnegie image tube with the R.C. spectrograph on 4 m Mayall telescope. Original dispersion 52 Å mm^{-1}, original scale perpendicular to the direction of dispersion 24″.6 mm^{-1}.

PETERSON *et al.* (*see* page 32)

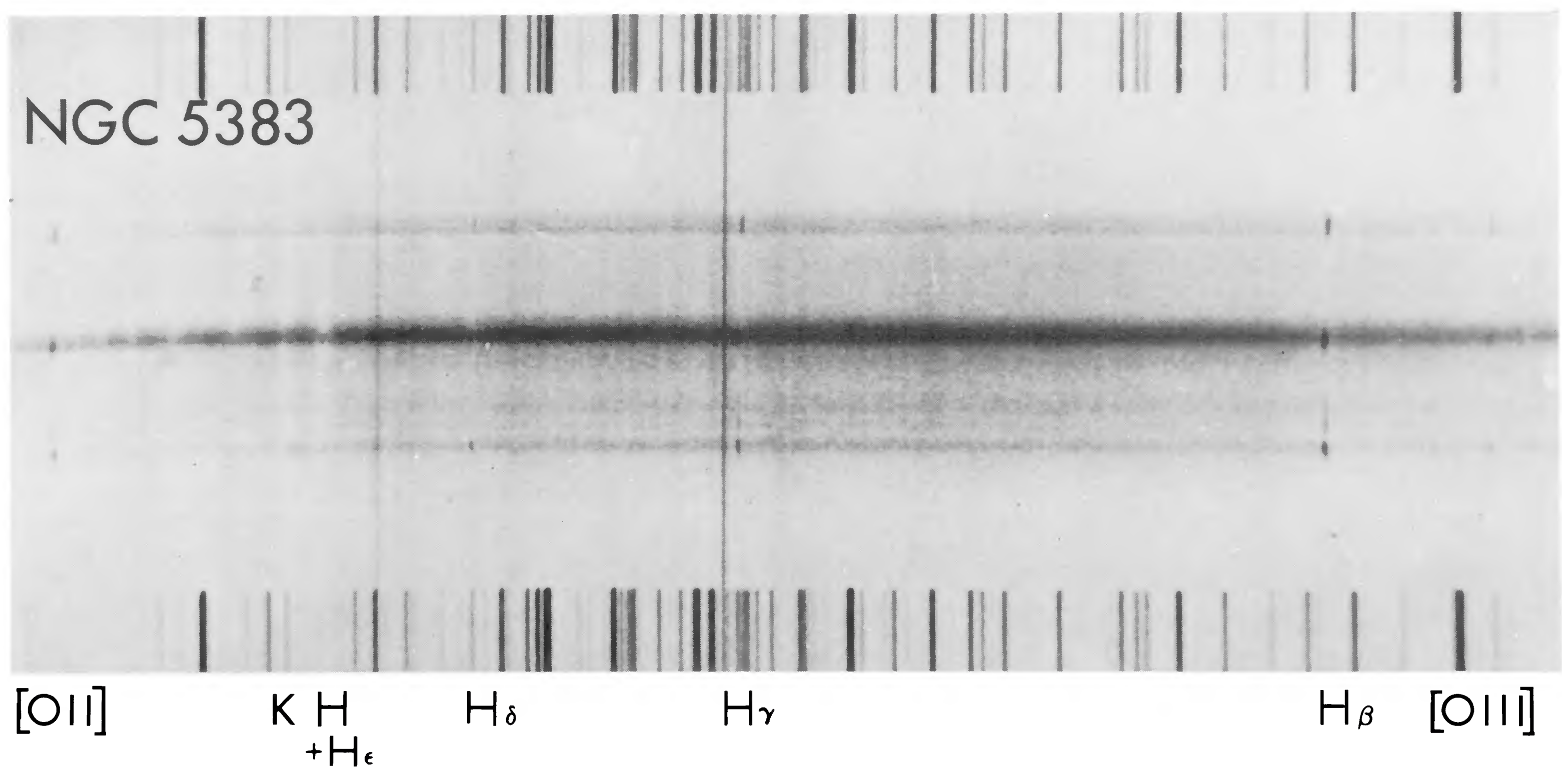

FIG. 3*b*.—Spectrum in blue, showing absorption and emission features; plate 811b, slit position 11, original dispersion 52 Å mm^{-1}, exposure 90 minutes. Note Hε in core of Ca II H absorption line.

PETERSON *et al.* (*see* page 32)